

The influence of stress history on the grain size and microstructure of experimentally deformed quartzite



Steven Kidder ^{a,*}, Greg Hirth ^b, Jean-Philippe Avouac ^c, Whitney Behr ^d

^a Department of Earth and Atmospheric Science, The City College of New York, 160 Convent Ave, New York, NY 10031, USA

^b Department of Geological Sciences, Brown University, Providence, RI 02912, USA

^c California Institute of Technology, MC 100-23, 1200 E. California Blvd, Pasadena, CA 91125, USA

^d Department of Geological Sciences, Jackson School of Geosciences, University of Texas, Austin, TX 78712, USA

ARTICLE INFO

Article history:

Received 9 April 2015

Received in revised form

4 December 2015

Accepted 11 December 2015

Available online 15 December 2015

Keywords:

Recrystallized grain size piezometry

Quartz

Dislocation creep

Microstructures

Rheology

EBSD

ABSTRACT

Deformation of middle crustal shear zones likely varies with time as a result of the stress build-up and release associated with earthquakes and post-seismic deformation, but the processes involved and their microstructural signature in the rock record are poorly understood. We conducted a series of experiments on quartzite at 900 °C to characterize microstructures associated with changes in stress and strain rate, and to investigate the feasibility of carrying out grain size piezometry in natural rocks that experienced analogous changes. Differential stress (referred to simply as “stress”) was varied in two-stage experiments by changing strain rate and by stopping the motor and allowing stress to relax. The two-stage samples preserve a microstructural record that can be interpreted quantitatively in terms of stress history. The microstructure associated with a stress increase is a bimodal distribution of recrystallized grain sizes. The smaller grains associated with the second deformation stage accurately record the stress of the second stage, and the surviving coarse grains remain similar in size to those formed during the earlier stage. The transient microstructure associated with stress decrease is a “partial foam” texture containing a larger concentration of stable 120° triple junctions than occur in samples deformed at a relatively constant strain rate. Our results indicate that microstructures preserved in rocks that experienced relatively simple, two-stage deformation histories can be used to quantitatively assess stress histories.

Grain growth rates during deformation are similar to rates observed in previous isostatic growth experiments, supporting theoretical approaches to recrystallized grain size, such as the wattmeter theory (Austin and Evans, 2007), that incorporate static growth rates. From an analysis of the experimental data for quartz recrystallized grain size, we find: 1) Recrystallized grain size quickly reaches a value consistent with ambient deformation conditions. We argue that this explains a good match between average grain sizes predicted by the wattmeter after complete recrystallization and the recrystallized grain sizes of the experiments. 2) The present formulation of the wattmeter overestimates the rates at which porphyroclasts recrystallize by as much as an order of magnitude, and 3) owing to problems with extrapolation of grain growth data for quartz, the wattmeter is not presently applicable to natural samples deformed at low temperatures. We present a simplified flow law for quartz, and suggest that the change in slope of the quartz piezometer at high stress (regime 1) is related to a switch to a linear viscous rheology.

© 2015 Elsevier Ltd. All rights reserved.

1. Introduction

Stress in the crust is traditionally viewed to be constant at a

* Corresponding author.

E-mail addresses: skidder@ccny.cuny.edu (S. Kidder), Greg_Hirth@brown.edu (G. Hirth), avouac@gps.caltech.edu (J.-P. Avouac), behr@utexas.edu (W. Behr).

given depth (e.g. Mercier et al., 1977; Brace and Kohlstedt, 1980; Kohlstedt et al., 1995). The existence of earthquakes and associated stress drops, and variations in pre- and post-seismic deformation (e.g. Bürgmann et al., 2002) however, make it clear that crustal stress magnitudes change with time. With the exception of pseudotachylites, the imprint that non-steady state deformation leaves on rocks is poorly understood and the processes involved are relatively unknown (e.g. Fagereng and Sibson, 2013). In this study,

we define non-steady state deformation broadly as deformation in which stress and strain rate vary substantially over time. While brittle deformation processes mainly accommodate non-steady state deformation at shallow crustal levels, microstructural studies on rocks from the Alpine Sesia Zone (Küster and Stöckhert, 1998; Trepmann and Stöckhert, 2001, 2003) indicate that ductile processes at deep crustal levels can also accommodate markedly non-steady state deformation (c.f. Handy et al., 2007).

Quartz plays a major role in controlling the rheology of the continental crust (e.g. Lowry and Pérez-Gussinyé, 2011), and quartz microstructures have proven to be useful records of numerous aspects of deformation history (e.g. Prior et al., 1990; Dunlap et al., 1997; Trepmann and Stöckhert, 2003; Mancktelow and Pennacchioni, 2004; Stipp et al., 2004; Fitz Gerald et al., 2006; Toy et al., 2008; Menegon et al., 2011; Bestmann et al., 2012). Interpretations of quartz microstructures often rely on laboratory deformation experiments (e.g. Hobbs, 1968; Means, 1989; Hirth and Tullis, 1992; Stipp et al., 2006), but there have been few experimental studies of non-steady state deformation in the ductile regime. Notable exceptions include “kick and cook” experiments (Trepmann et al., 2007; Druiventak et al., 2012), which investigate the microstructural changes associated with annealing following a large stress pulse. Very few studies have addressed the grain-scale microstructures associated with stress changes during dislocation creep (Ross et al., 1980; Van der Wal et al., 1993; Austin and Evans, 2009). The lack of experimental results makes it difficult to assess the degree to which exhumed rocks were affected by non-steady state deformation.

Non-steady state deformation has the potential to affect recrystallized grain size. In steady state experiments on quartz (and other minerals), recrystallized grain size is strongly correlated with differential stress (Stipp and Tullis, 2003), and recent work demonstrates that the experimental relationship is accurate at geologic conditions (Kidder et al., 2012). Studies involving recrystallized grain size piezometry often focus on the finest recrystallized grains formed near the brittle–ductile transition since these grains are best preserved and provide a constraint on peak crustal stress (e.g. Weathers et al., 1979; Ord and Christie, 1984; Dunlap et al., 1997; Stipp et al., 2002; Fitz Gerald et al., 2006; Behr and Platt, 2011; Kidder et al., 2012). These stress estimates have different meanings depending on whether they are interpreted to represent constant stress or transient and decaying stresses following earthquakes (e.g. Trepmann and Stöckhert, 2003).

We present the results of a laboratory investigation of non-steady state behavior of quartz during ductile deformation. We compare the rheology and microstructures of nearly constant strain rate experiments and experiments where strain rate, and consequently differential stress (referred to below simply as “stress”), experienced a major change. These first attempts at investigating non-steady state behavior in quartz during dislocation creep allow us to address a number of open questions: can we distinguish microstructural features developed during steady vs. non-steady state deformation? How much deformation is required to obscure microstructures developed during earlier stages of deformation? Under what conditions, if any, can recrystallized grain size piezometry be applied to samples that have experienced non-steady state deformation? What are the kinetics and mechanisms of grain size change during deformation? We additionally investigate the applicability of the wattmeter (e.g. Austin, 2011) to predict sizes and rates of change of grain size.

2. Background

The term dynamic recrystallization refers to changes in grain size, shape and orientation driven by strain energy in the form of

dislocations (Poirier and Guillope, 1979; Stünitz, 1998). During dynamic recrystallization the formation of new grains reduces internal strain energy associated with elevated dislocation density. Recrystallized grains are thought to form by two major processes: grain-boundary migration and subgrain rotation recrystallization (e.g. Urai et al., 1986). In experimentally deformed quartz, three dislocation creep regimes have been identified (Hirth and Tullis, 1992). At high stress levels (regime 1), new grains form predominantly by the migration or “bulging” of grain boundaries in response to large, intergranular dislocation density differences. Bulges are pinched, rotated or sheared off, thereby forming new grains (e.g. Stipp and Kunze, 2008). At moderate stress (regime 2), formation of new grains is dominated by rotation recrystallization: dislocations combine into lower energy subgrain boundaries, and misorientation increases until high-angle grain boundaries form. At low stress (regime 3), grain-boundary mobility increases and recrystallized grains form by both grain-boundary migration recrystallization and subgrain rotation recrystallization. While the dominance of subgrain rotation and grain-boundary migration recrystallization differs in the three regimes, both processes occur to some extent in all three regimes (e.g. Stipp and Kunze, 2008).

Previous experimental work on quartz indicates that the relationship between stress and recrystallized grain size (Fig. 1) is independent of temperature and water content (Bishop, 1996; Stipp and Tullis, 2003; Stipp et al., 2006). No previous experimental studies have investigated the role of changing stress on recrystallized grain size in quartz; however, such transient effects have been analyzed in other materials and natural samples. For example, Ross et al. (1980) deformed olivine under increasing and decreasing stress levels and found that recrystallized grain sizes respond in “minimal” (but unspecified) strains and times. Van der Wal et al. (1993) found that the adjustment period for olivine occurs within 3–10% strain for modest stress decreases. White et al. (1985) deformed impure magnesium to high strains and found that recrystallized grain size within shear zones in the samples remained at peak stress levels despite strain weakening. Recrystallized grains in zones bordering the shear zones however equilibrated to the new stress conditions. In experiments on calcite, Austin and Evans (2009) found that fine-grained aggregates grew during diffusion creep at the same rates that occur under isostatic conditions. Prior et al. (1990) and Cross et al. (2015) quantified rates of change in grain size associated with the deflection of quartz about porphyroclasts in a natural shear zone.

3. Methods

3.1. Experimental methods

Experiments were conducted in two modified Griggs apparatuses (Tullis and Tullis, 1986) on beige-colored Black Hills Quartzite (6.3 mm diameter, 14 mm length). The quartzite is >99% pure quartz with a grain size of ~70 μm (Stipp and Kunze, 2008). The material has no lattice preferred orientation and grains exhibit minimal or no deformation microstructures. Samples consisted of two stacked cylinders of quartzite with 0.2 weight percent water added between the pieces. Platinum jackets were annealed for 15 min at 900 °C and folded over annealed platinum disks on each end of the samples. The platinum-encased samples were inserted into a Ni sleeve and NaCl assembly identical to that described by Chernak et al. (2009). Samples were brought to pressure along a standard pressure-temperature path following Chernak et al. (2009); at 300 °C and a confining pressure of ~1.3 GPa, the deformation piston was advanced to hit the sample (i.e., a “cold hit”), and then retracted. Temperature was then increased to 900 °C where it was held for ~12 h prior to the initiation of uniaxial compression.

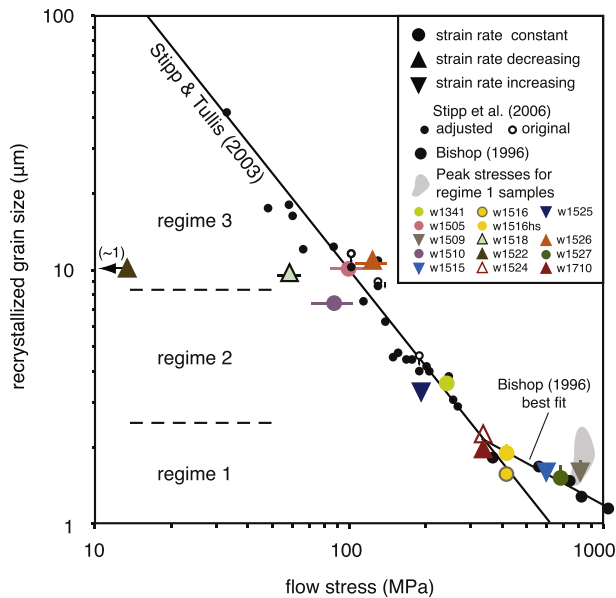


Fig. 1. Plot of recrystallized grain size vs. stress showing the characteristic inverse correlation in the data from previous studies (black symbols from Bishop, 1996; Stipp and Tullis, 2003; Stipp et al., 2006) and our experiments (colored symbols). Plotted stresses are either averages over the interval between 10% strain and the final stress, or final stresses for samples in which stress was changing significantly at the end of the experiment (see Table 1). For purposes of comparison, the piezometer line and Stipp data are adjusted slightly towards smaller grain size based on a reanalysis using our EBSD grain-size routine of three samples from Stipp and Tullis (2003). The original positions of the three samples are plotted for reference as open circles. A readjustment of the older grain-size data determined from optical images toward smaller sizes is supported by a detailed EBSD-based reanalysis of the original samples by Cross, Prior and Stipp (in prep.). The small grey blob indicates the peak stresses experienced by the fine-grained samples (experiments w1509, w1515, w1516, w1524, w1527, and w1710). Error bars are standard errors of grain size data (most smaller than the plotted data points) and the standard deviation of stress experienced during the period over which stress was averaged. Where final stresses are plotted, no such statistic is possible. The clustering of our new data along the piezometer indicates good overall reproducibility between the various experiments, and a lack of importance of earlier deformation history on the final recrystallized grain size of most samples.

Two exceptions to this were experiments w1341 and w1524, in which deformation was imposed immediately after the sample reached 900 °C. The motivation for annealing samples at high temperature before deformation was to facilitate equilibration of the samples with respect to water content. The experiments were conducted at strain rates of approximately 10^{-4} or 5×10^{-5} (regime 1), 10^{-5} (regime 2), and 10^{-6} s^{-1} (regime 3 near the regime 2–3 boundary). Two-stage experiments were conducted with either an increase or decrease in strain rate after 20–30% axial strain. In one experiment (w1522), the motor was shut off after regime 1 deformation and stress was allowed to relax at 900 °C. Mechanical data were processed assuming that the samples remained constant-volume cylinders. Friction corrections were made following Getsinger and Hirth (2014), i.e. with secondary corrections applied to the second stages of the two stage experiments. Further information on the starting material and procedures for processing the mechanical data can be found in the references given by Chernak et al. (2009). Differential stress versus axial strain data for the experiments is plotted in Fig. 2.

3.2. Grain size analyses

Preparation of the samples for grain size analysis involved polishing with a $\frac{1}{4} \mu\text{m}$ diamond compound before a final vibropolish for $\sim 8 \text{ h}$ in a $0.05 \mu\text{m}$ Al or colloidal Si suspension. Electron

backscatter diffraction (EBSD) maps were made on uncoated samples with the Zeiss 1550VP field emission Scanning Electron Microscope (SEM) equipped with an Oxford Instruments EBSD system at Caltech and a similar SEM at the University of Otago. Patterns were acquired using the *Flamenco* software at a working distance of 10 mm, an accelerating voltage of 20 kV, step size between 0.15 and $0.5 \mu\text{m}$, 70° sample tilt, 7 nA beam current, and chamber pressure of 15 Pa.

Noise reduction involved first removing single points with orientations not shared by neighbors (“wild spikes”). Further, when six or more neighboring pixels had the same orientation, the non-indexed pixels were iteratively filled with the average orientation of neighbors. Grains were identified automatically with the CHANNEL 5 software using a misorientation angle of $>10^\circ$ to define grain boundaries (White, 1977). Misorientations of $60 \pm 5^\circ$ about [001] were considered to be Dauphine twins rather than grain boundaries. As described by Kidder and Prior (2014), to minimize the effects of beam damage in EBSD maps at small step size, we scanned down the samples (opposite the conventional direction). A more detailed description of the grain-size analysis routine is given in the supplemental material.

Grain size is defined as the diameter of a circle with an area equivalent to that measured. Following Stipp and Tullis (2003), no stereological correction was applied and grain sizes were calculated as root mean square averages. Median values are also reported in Table 1 as these provide a more robust measure of central tendency for recrystallized populations (Ranalli, 1984; though see also approach of Lopez-Sanchez and Llana-Funez, 2015). Because of the extremely high resolution needed to accurately distinguish fine recrystallized grains, the EBSD maps of the regime 1 and 2 samples contain insufficient coarse grains to calculate meaningful estimates of average grain size (unrecrystallized plus recrystallized grains). To estimate the average grain size in these samples, we measured linear intercepts with an optical microscope. The lengths between each grain boundary were measured, and root mean square averages calculated both parallel and perpendicular to the Z direction were averaged. Fine-grained areas where grain boundaries cannot be resolved optically were populated with line intercept measurements of equal length from recrystallized areas of the EBSD maps. Table 1 reports statistics for both average and recrystallized grain size. Histograms of the grain size data from the EBSD maps are given in the supplemental material. To distinguish between recrystallized and relict grains in the EBSD maps, we chose size cut-off values based on textural criteria: unrecrystallized grains tend to have heterogeneous band contrast due to large amounts of internal distortion (e.g. Figs. 3 and 4) and irregular or elongate shapes. While in some cases the distinction can be made very easily (e.g., Fig. 3), in most samples the origin of many grains is not obvious. For the sake of simplicity and repeatability, we defined recrystallized grains as the grains with sizes less than $20 \mu\text{m}$, except in samples ending in regime 1 where a cutoff of $5 \mu\text{m}$ was used.

4. Results

4.1. Mechanical data

As previously described (Hirth and Tullis, 1992), quartzite deformed in regime 1 first exhibits significant strain hardening, followed by strain weakening after recrystallization initiates at $\sim 15\%$ strain. The regime 1 experiments generally follow similar stress–strain curves (Fig. 2), indicating that deformation conditions were reproducible and consistent among the experiments. Two exceptions to this are experiment w1509, which was conducted at a higher strain rate of $\sim 10^{-4} \text{ s}^{-1}$ and w1524, which was conducted with constant furnace power—but un-measured temperature—after

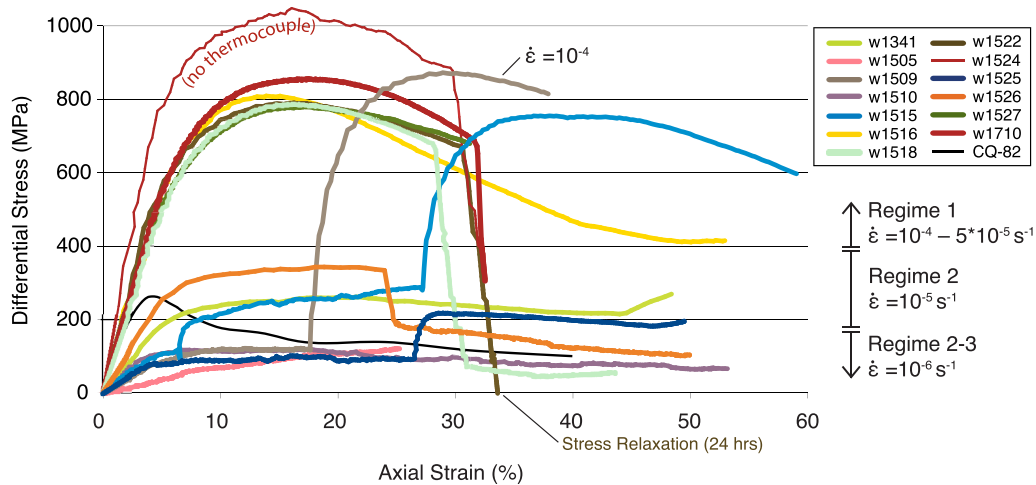


Fig. 2. Differential stress vs. axial strain for the experiments. Labels on the right side of the plot show approximate strain rates for the experiments and equivalent quartz deformation regimes (Hirth and Tullis, 1992). The thin black curve is a regime 3 experiment from Hirth and Tullis (1992). The abrupt apparent increase in strength of w1341 at ~45% strain is believed to be due to frictional contact of the σ_1 piston with the σ_3 piston (Chernak et al., 2009).

a thermocouple failure. Most samples deformed at regime 2 and regime 3 conditions experienced relatively constant flow stresses after 5–10% strain.

We note a good overall consistency of our results with Stipp and Tullis' (2003) data acquired using the molten salt cell (Fig. 1). This confirms Gleason and Tullis' (1993) observation that little systematic difference exists between stress values determined using the solid salt cell and molten salt cell at the high temperatures of our experiments. In experiments with abrupt strain rate changes, the eventual flow stresses are similar to those observed in single-stage experiments. For example, experiment w1515 first experienced regime 3 (low strain rate) deformation but later reached a peak stress at regime 1 conditions similar to that observed for the other samples deformed at the same high strain rate ($5 \times 10^{-5} \text{ s}^{-1}$; w1516, w1522, w1527, w1710). Similarly, the behavior of w1525 after switching from regime 3 to regime 2 conditions is nearly identical to the high strain portions of the regime 2 experiment w1341.

Table 1 summarizes the experimental conditions and results for each experiment. The stresses reported in Table 1 (and plotted in Fig. 2) are final stresses for experiments where stress was changing significantly at the end of the experiment. For the remaining experiments, we follow Stipp and Tullis (2003) and report average stress values over the interval between 10% strain (from the beginning of one-stage experiments or after the strain rate switch in two-stage experiments) and the final stress. In one experiment (w1515), we increased confining pressure slightly (from ~1.41 to 1.48 GPa) at a strain of ~7% to bring it to a value consistent with the other experiments. This coincided with a significant increase in recorded stress lasting for (at least) the duration of the first stage of the experiment. Higher pressures in quartzite weaken quartz within time scales much shorter (<~3 h; Holyoke and Kronenberg, 2013) than the apparent strength increase sustained during the experiment (~38 h). Thus, we attribute the rise in strength to a frictional effect on the piston rather than a true change in the stress experienced by the sample.

4.2. Microstructural observations

In experiments where strain rate was not abruptly changed, microstructures (Figs. 5a, 6a and 7a) are indistinguishable from those previously described by Hirth and Tullis (1992). In experiments involving a strain rate increase to regime 1 conditions,

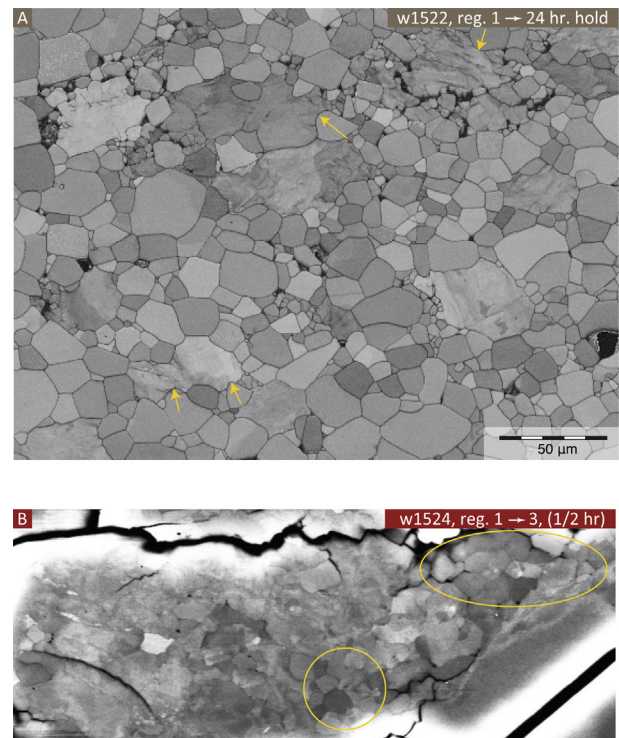


Fig. 3. Microstructures of two samples switched from high stress (regime 1) to low stress. A. Band contrast image of sample w1522 (left for 24 h at 900 °C with the motor off). The prevalence of ~120° triple junctions and straight or gently curved grain-boundary segments is indicative of grain growth driven by grain-boundary surface energy minimization. Locally, large differences in dislocation density between new grains (grains with uniform fill) and remnants of unrecrystallized relict grains (grains with uneven fill) drove grain-boundary migration (arrows). Contrast has been increased in the image for illustrative purposes. B. Orientation contrast image of sample w1524 which spent ~30 min at regime 3 conditions following deformation in regime 1. New grains showing straight grain boundaries and 120° triple junctions are present, suggesting grain-boundary energy driven grain-growth (areas indicated in yellow). The patchy microstructure in much of the figure is typical of highly distorted regime 1 quartz. σ_1 is vertical in both images (For interpretation of the references to color in this figure legend, the reader is referred to the web version of this article.).

coarser recrystallized grains remaining from the regime 3 stage are deformed and overprinted by finer grains. The remnant grains are easily distinguishable after 20% strain in regime 1, but are reduced

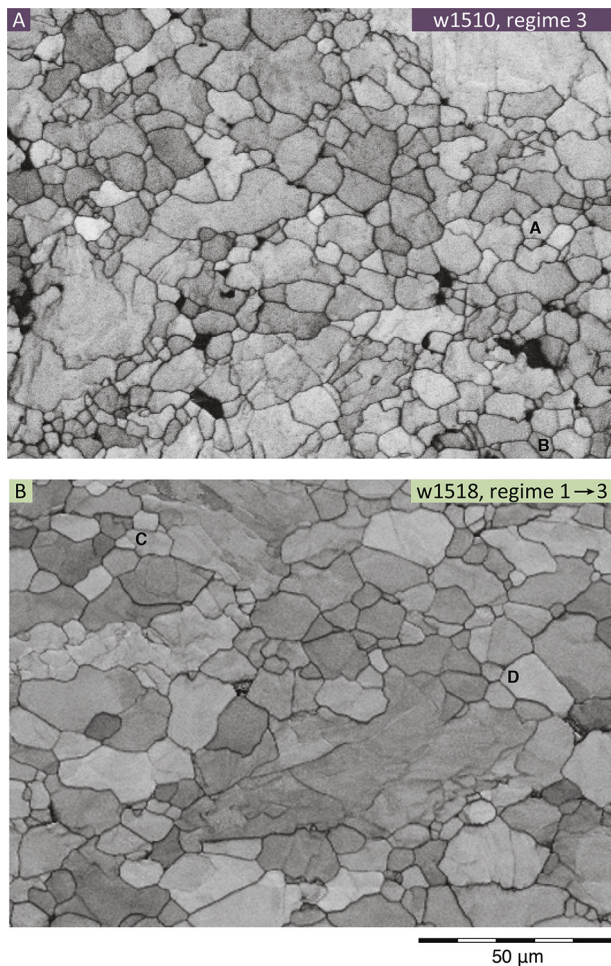


Fig. 4. Comparison of band contrast images from two samples that experienced a final deformation stage involving $\sim 25\%$ strain at regime 3 conditions. A. Sample w1510 was deformed entirely in regime 3 and had achieved a stable recrystallized grain size. B. Sample w1518 experienced $\sim 25\%$ strain in regime 1 followed by deformation at regime 3 conditions. Recrystallized grain size in sample w1518 increased by nearly an order of magnitude during the second stage of the experiment, and its microstructure is characterized by patches containing gently-curved grain boundaries and $\sim 120^\circ$ triple junctions (e.g. to the left of grains C and D). Similar patches also occur in w1510, e.g. near grains A and B, but are less abundant. These microstructures suggest that grain-boundary energy reduction: 1) drives grain growth following major changes in stress (panel B), and 2) is involved in maintaining recrystallized grain size during steady state deformation (panel A). σ_1 is vertical in both images.

in number and less conspicuous by 32% strain (Fig. 5). Microstructures in a sample (w1525) deformed at regime 2 conditions to a strain of $\sim 23\%$ after an early stage of regime 3 deformation show only minor differences relative to a sample deformed entirely within regime 2 (Fig. 6). In experiments where strain rate was decreased to regime 3 conditions, earlier higher stress fabrics evolve into a coarser-grained microstructure with a grain size similar to that observed in single-stage regime 3 experiments (Fig. 7). Two-stage samples that experienced an initial period of regime 1 deformation (w1518, w1522) are more recrystallized than comparably strained samples that experienced only regime 3 deformation (w1505, w1510).

Two-stage experiments w1518, w1522, w1524 and w1710, in which strain rate was decreased after achieving $\sim 30\%$ strain in regime 1, show aspects of a foam texture associated with the switch to lower stress deformation. Sample w1522, which underwent stress relaxation (motor off) for 48 h, is dominated by a foam texture comprising 120° triple junctions and straight or gently curved grain boundaries (Figs. 3a and 7d). While this

microstructure is considered clear evidence of grain-boundary energy driven grain-growth (e.g. Platt and Behr, 2011), microstructures indicative of strain-induced grain-boundary migration—grain boundaries convex into “hardened” original grains—are also evident (Fig. 3a). Experiments w1524 and w1710 underwent only ~ 30 min of subsequent low-stress deformation in regime 3, but show patches dominated by 120° triple junctions (Fig. 3b). Similar “annealed” areas are not evident in samples quenched during regime 1 deformation. Following a regime 1 stage, sample w1518 underwent $\sim 10\%$ strain (~ 24 h) under regime 3 conditions. While having a recrystallized grain size similar to the single stage regime 3 samples (w1505 and w1510), this sample also has a high concentration of 120° triple junctions (Figs. 4 and 7). To quantify this observation, we visually inspected ~ 200 triple junctions in samples w1510 and w1518. To avoid subjective sampling,

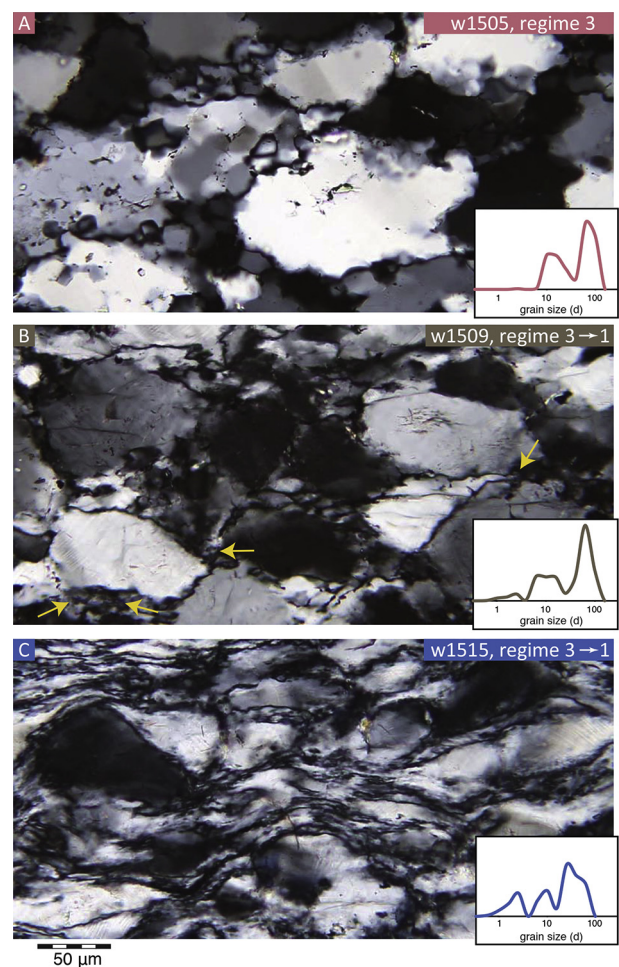


Fig. 5. Photomicrographs showing sequential overprinting of low stress (regime 3) fabric by regime 1 deformation. A: sample w1505 was deformed to $\sim 25\%$ strain in regime 3. B: sample w1509 underwent $\sim 18\%$ strain in regime 3 then just began to recrystallize under regime 1 conditions ($\sim 20\%$ strain at 10^{-4} s^{-1}). Relict grains of size $\sim 10 \mu\text{m}$ survive from the early regime 3 stage. The finer grains are not clearly distinguishable at this scale due to their small size ($\sim 1 \mu\text{m}$) but the locations of some patches of fine-recrystallized grains are indicated by arrows. C: sample w1515 underwent $\sim 27\%$ strain in regime 3, then $\sim 32\%$ strain at $5 \times 10^{-5} \text{ s}^{-1}$. Fine recrystallized grains are much more common. Large ribbon grains ($\sim 10 \mu\text{m}$) may represent either highly deformed grains from early deformation or may have formed during regime 1 deformation (they also occur in samples that only experienced regime 1 deformation such as w1524 and w1710). The histograms were made using a linear intercept method in the areas shown, and depict the relative concentrations of original grains and recrystallized grains from the two deformation stages. The y-axis on the histograms is the normalized number of grains \times grain size. σ_1 is vertical in all images. High-resolution, larger-area versions of these images are available as Virtual Microscope eSlides VM02409, VM02410, and VM02411.

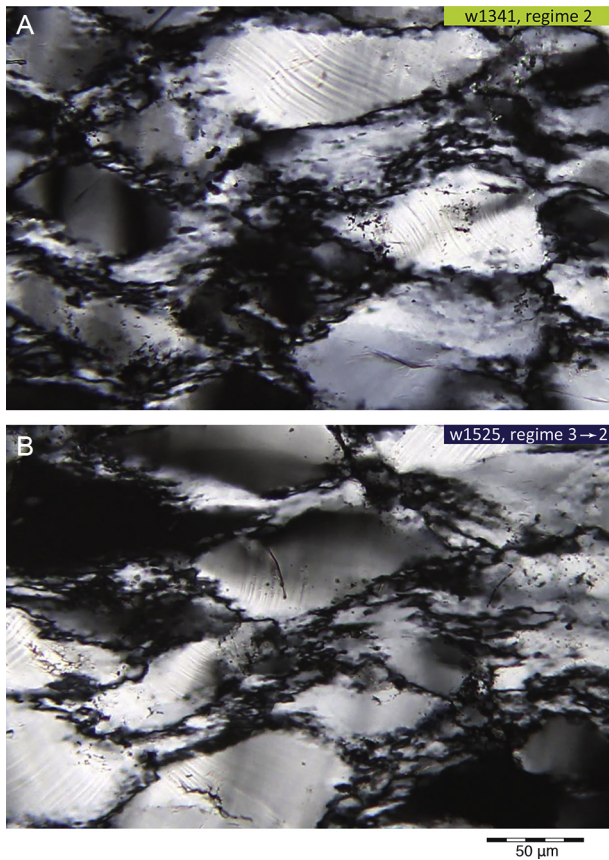


Fig. 6. Photomicrographs of the two samples that ended at regime 2 conditions. A: Sample w1341, deformed in regime 2 throughout an entire experiment. B: Sample w1525, ~27% strain in regime 3 followed by deformation at regime 2 conditions. The resulting fabrics are similar although w1341 appears to contain more subgrains and fewer large (~10 µm) recrystallized grains. σ_1 is vertical in both images. High-resolution, larger-area versions of these images are available as Virtual Microscope eSlides VM02412 and VM02413.

analysis areas were randomly selected from the images in Fig. 4 and all triple junctions in these areas were inspected. In w1510 and w1518, 24% and 42%, respectively, of triple junctions qualitatively “look” like stable 120° triple junctions. This suggests a significant difference exists between the two fabrics, with w1518 having a microstructure more similar to a foam texture. We refer to such microstructures as “partial foam” textures.

4.3. Lattice preferred orientation

Stereonets of c- and a-axis orientations (provided in supplementary material) show little difference in lattice preferred orientation (LPO) associated with the different stress histories experienced by the samples. “Pole plot” histograms produced by counting the numbers of grains that fall within small circle girdles at 5° increments (e.g. Gleason et al., 1993), however, reveal that the samples where significant grain growth occurred have greater concentrations of grains in “hard” orientations with respect to σ_1 (Fig. 8). Gleason et al. (1993) made a similar observation in samples of flint that were deformed during grain growth and dynamic recrystallization at regime 2 and 3 conditions.

4.4. Recrystallized grain size

Fig. 1 shows the relationship between mean recrystallized grain size and stress for the experiments. The empirically derived recrystallized grain-size piezometer for quartz (Bishop, 1996; Stipp

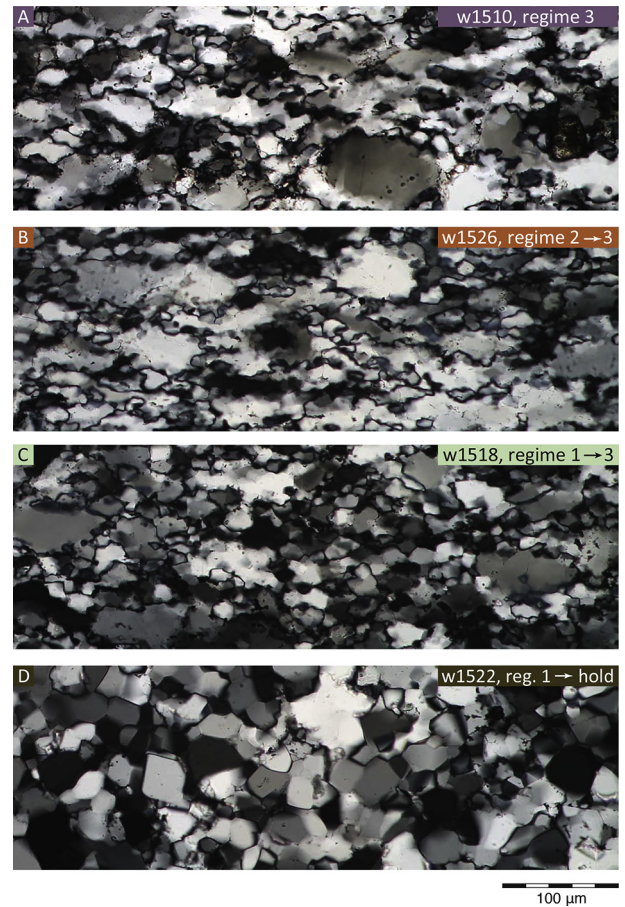


Fig. 7. Photomicrographs of samples from four experiments ending at low stress. The samples in panels A, B and C were deformed in regimes 3, 2, and 1, respectively, during an early stage of deformation but all ended with ~25% strain at regime 3 conditions. Sample w1522 (D) was deformed in regime 1 before annealing with the motor off for 24 h. The microstructures in (A) and (B) are difficult to distinguish from one another despite their different deformation histories. Sample w1518 (C) was undergoing grain growth during deformation when quenched and has a microstructure more similar to sample w1522 (D). σ_1 is vertical in all images. High-resolution, larger-area versions of these images are available as Virtual Microscope eSlides VM02414, VM02415, VM02416, and VM02417.

and Tullis, 2003) is also plotted in Fig. 1 along with experimental data used in its calibration (small black circles). The position of the recrystallized grain size data relative to the piezometer is not a function of strain (Fig. 9). With one exception, the data from our study fall close to the piezometer, even for the experiments in which stress changed significantly. This observation indicates that, in general, recrystallized grain size adjusted within the time period and cumulative strains of the second stages of the experiments. The data point in Fig. 1 that falls far from the piezometer is the stress-relaxation experiment (w1522). In this experiment, grain growth was unable to keep pace with a stress lowered to nearly isostatic conditions.

The highest strain sample (w1516, regime 1) contains a localized deformation zone similar, but less developed, than a zone described by Stipp and Kunze (2008). We measured grain sizes both within this zone and outside it, toward the sample center (locations of the two EBSD maps are shown in the supplementary material). The difference in recrystallized grain size (~20% larger in the shear zone) significantly exceeds the uncertainty of the mean grain size estimate for each map (Table 1) and is opposite the difference noted by White et al. (1985) in impure magnesium. More subtle internal variations in grain size were also observed (Fig. 10).

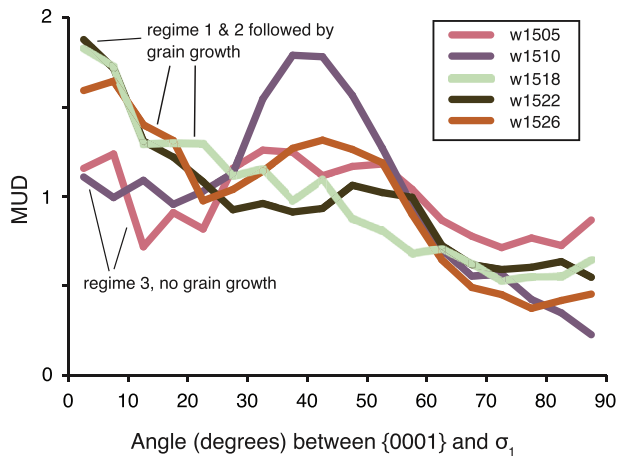


Fig. 8. Pole plots for samples ending at low stress. Compared to the regime 3 samples (w1505 and w1510), the three samples that experienced significant grain growth (w1518, w1522 and w1526) show significantly higher Multiples of Uniform Density (MUD) for c-axes oriented at a small angle to σ_1 , a “hard” orientation. The similarity in the pole plots for the grain growth samples suggests the operation of the same growth process both during deformation (w1518 and w1526) and after (w1522). Gleason et al. (1993) observed similar patterns and postulated that grains with hard orientations were favored for growth because they contain fewer dislocations than typical grains. MUD values were calculated using the Channel 5 Mambo software on 250 randomly selected grains and are smoothed using a rolling average of adjacent values.

4.5. Predicted grain size

Grain size measurements are compared to predicted grain sizes in Fig. 11. The Stipp and Tullis (2003) piezometer predicts the experimental results reasonably well for grain sizes $>2 \mu\text{m}$. This outcome is expected because the Stipp and Tullis (2003) piezometer is a best-fit line to experimental data similar to that generated here. Regime 1 data (Bishop, 1996) were acquired from experiments on a fine-grained starting material (novaculite), with grain size measurements made on etched boundaries in a SEM. Stipp and Tullis (2003) noted that these data fall off the trend of their piezometer (e.g. Fig. 1). Our results for regime 1 samples follow the same trend as that from Bishop (1996; Figs. 1 and 11) demonstrating that the change in trend is not a result of differences in experimental material, grain size measurement technique, or initial

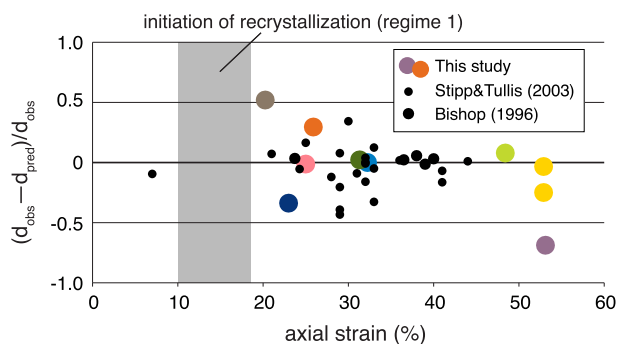


Fig. 9. Axial strain versus the normalized difference between observed recrystallized grain size (d_{obs}) and the recrystallized grain size predicted by the Stipp and Tullis (2003) or Bishop (1996) piezometers (d_{pred}). For two-stage stress-increase experiments, strains plotted are for the second portion of the experiment. Samples with foam textures are not plotted. Data in the graph lack a systematic trend and we infer that recrystallized grain size is mainly a function of ambient stress rather than stress history or degree of recrystallization. The lack of a trend supports the use of steady state grain-size values from relationships such as the wattmeter to predict recrystallized grain sizes in partially recrystallized rocks.

grain size.

While several theoretical grain size–stress relationships have been proposed (e.g. Twiss, 1977; Edward et al., 1982; Derby and Ashby, 1987; Derby, 1990; De Bresser et al., 1998; De Bresser et al., 2001; Hall and Parmentier, 2003; Austin and Evans, 2007; Shimizu, 2008; Rozel et al., 2011; Hackl and Renner, 2013), we focus here on testing the recently developed wattmeter model (Austin and Evans, 2007, 2009) because of its relative simplicity and ability to predict not just steady state grain size, but grain size evolution, such as experienced in our samples. The wattmeter models a dynamic balance between the rates of grain growth based on static grain growth experiments and grain size reduction. It assumes that: 1) a fraction (λ) of the mechanical work rate during dislocation creep (stress \times strain rate) is not dissipated as heat, but rather results in increased internal energy due to changes in the microstructure; and 2) the rate of grain size reduction is proportional to this rate of change of internal energy. The resulting relationship for the rate of change in grain size is (Austin and Evans, 2009):

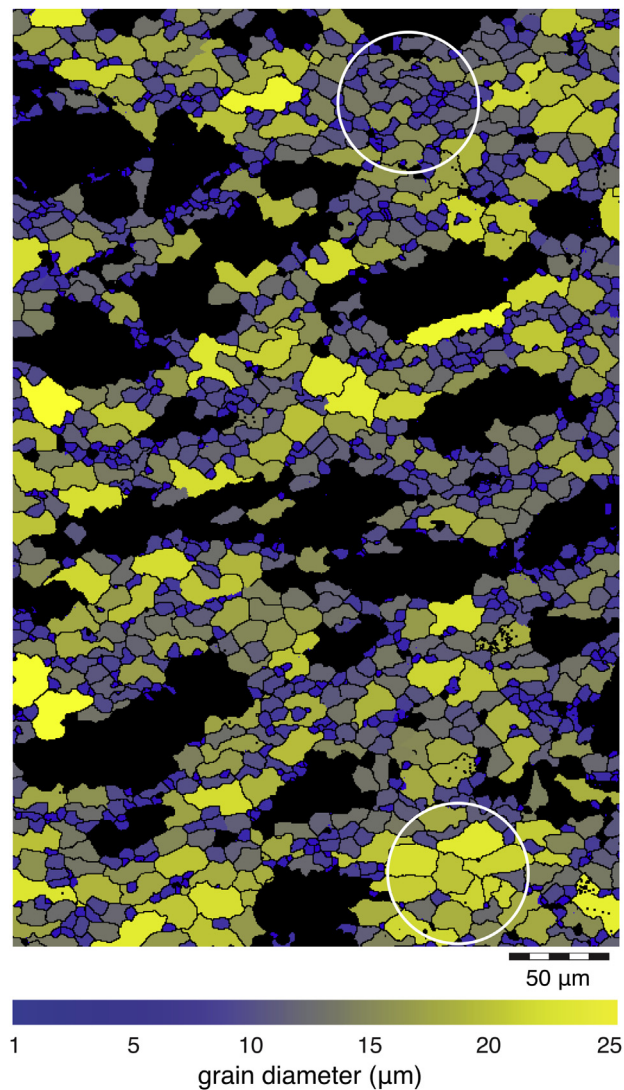


Fig. 10. EBSD map from sample w1510 colored by grain size. Grains of size $>25 \mu\text{m}$ and void space are black. Note that the spatial distribution of grains of various sizes is non-random. Smaller and coarser grains tend to cluster (e.g. the two circled areas). σ_1 is vertical.

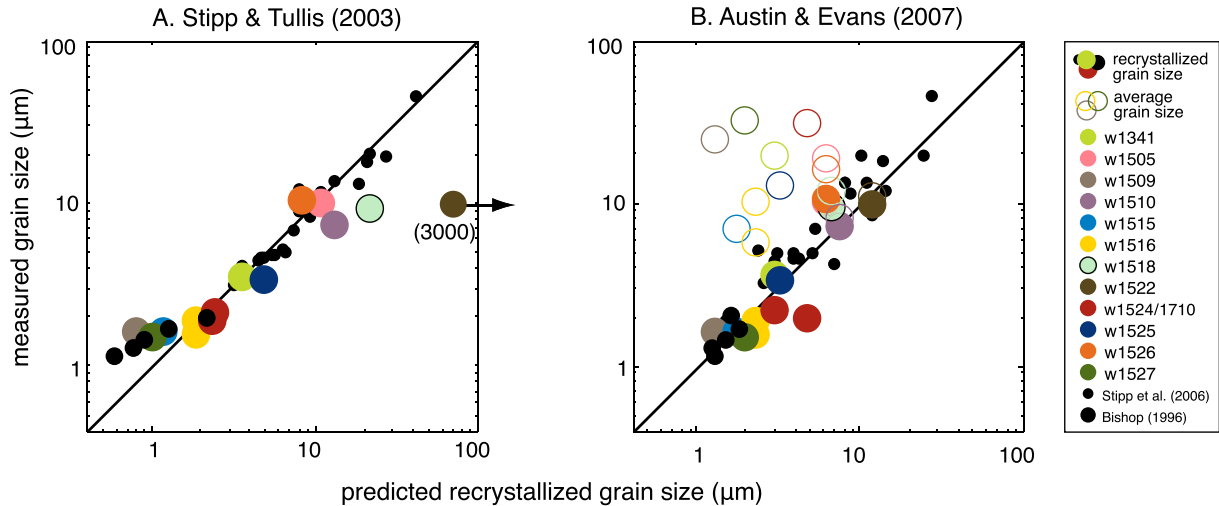


Fig. 11. Measured grain sizes vs. grain sizes predicted by A) Stipp and Tullis (2003), and B) the wattmeter (Austin and Evans, 2007). Recrystallized grain sizes are plotted as filled dots, average grain sizes (recrystallized grains plus relict grains) are shown as open symbols for our data but are not available for the older datasets. Although intended to predict average grain size, the wattmeter instead provides values that match recrystallized grain size, including the high stress data (which deviate from the 1:1 line in A).

$$\dot{d} = K_g \exp \left[\frac{-Q_g}{RT} \right] p^{-1} d^{1-p} - \frac{\beta \lambda \sigma \dot{\epsilon} d^2}{\pi \gamma} \quad (1)$$

where d = average grain size, R = gas constant, T = temperature (K), $\dot{\epsilon}$ = strain rate, σ = differential stress, γ = grain-boundary energy, β = fraction of the total mechanical work rate accommodated by dislocation creep, p = grain growth exponent, K_g = grain growth pre-exponential factor, and Q_g = grain growth activation enthalpy. We assume $\lambda = 0.1$ following Austin and Evans (2007,

2009) and $\beta = 1$ based on slow rates of diffusion creep observed in pure quartz aggregates (2004). For the grain growth parameters, we used the values determined by Wightman et al. (2006) from the experimental data of Yund and Tullis (1982). We use a numerical solver to track the predicted grain-size evolution of the samples based on the experimental stress and strain data. This treatment is advantageous because (1) it can be used to predict grain size evolution rates and (2) *a priori*, it is unknown whether sufficient deformation has occurred to reach a steady-state grain size. The code used in the calculations is provided in the supplemental material. Fig. 12 shows predicted grain size evolution curves.

We emphasize that the wattmeter, as presented by Austin and Evans (2007, 2009), predicts average grain size, i.e. the average (grain-boundary area/unit volume) of both recrystallized and non-recrystallized grains. As shown with the open circles in Figs. 11b and 12, the wattmeter poorly predicts this aspect of the grain-size populations, especially for the higher stress samples. However, the average grain sizes predicted by the wattmeter correspond closely to the observed recrystallized grain sizes, even for samples that fall off the prediction of the Stipp and Tullis (2003) piezometer due to the break in slope in the piezometer at high stresses/small grain sizes or incomplete grain growth following high stress deformation (Fig. 11). This is considered further in the Discussion. While the wattmeter significantly overestimates grain-size reduction rates (Fig. 12), it captures grain growth rates during the experiments well. The sizes of recrystallized grains that experienced significant growth (w1518, w1522) fall near the predictions of both the wattmeter and the static growth relationship (Wightman et al., 2006, Fig. 12).

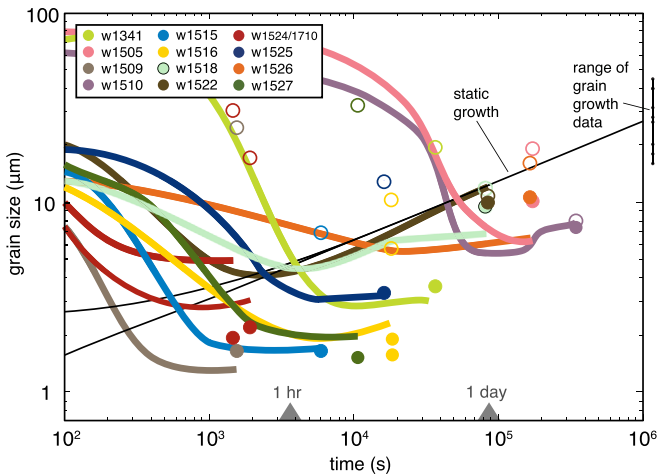


Fig. 12. Grain size evolution predicted by the wattmeter for each experiment. Recrystallized grain sizes are shown as filled circles and average grain size data as hollow symbols. For two-stage experiments, the starting point on the plot is an estimated average grain size at the start of the second deformation stage based on data from other experiments (Table 1). Comparison of the predicted grain size evolution paths with the measured average grain size data demonstrates that the wattmeter significantly overestimates grain size reduction rates. Thin black lines show grain growth predictions for isostatic conditions (Wightman et al., 2006) for two initial grain sizes—note that these are similar to the predictions of the wattmeter during grain growth after minimum grain size is reached (e.g. at ~3000 s for w1518 and w1522). The range of the static grain growth data for novaculites (Fig. 4a of Tullis and Yund, 1982) relative to the Wightman et al. (2006) predictions is shown on the right side of the graph to illustrate the similar scatter of that dataset. Differences between the wattmeter predictions and recrystallized grain size data are small enough to be explained by typical random differences in growth rates from sample to sample.

5. Discussion

5.1. Implications for grain size piezometry

A common concern with recrystallized grain size piezometry is that it may be difficult to detect whether natural deformation occurred at a microstructural or mechanical steady state. It is often assumed that steady state conditions are required for grain size piezometry (e.g. Twiss, 1977; Christie and Ord, 1980; Kenkmann and Dresen, 1998; Trepman and Stöckhert, 2003; Stipp et al.,

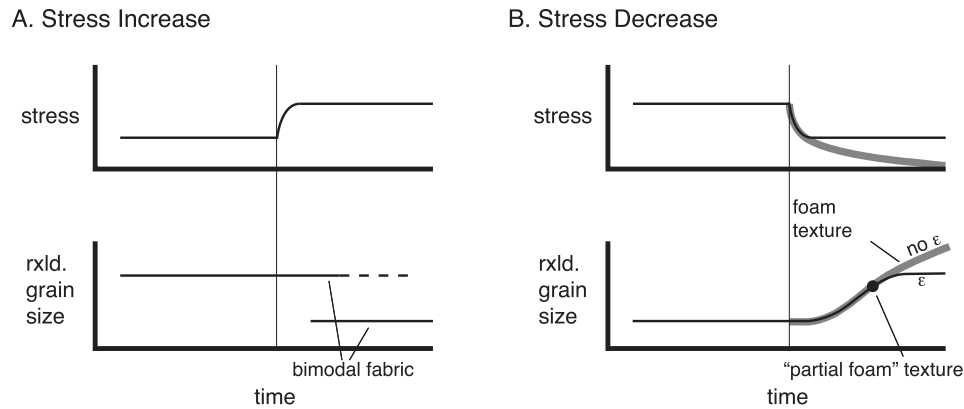


Fig. 13. Diagrams summarizing grain size evolution of samples experiencing switches to (A) and from (B) higher stress deformation. A. Samples experiencing a stress increase have bimodal recrystallized grain size distributions (e.g. Fig. 5). Both grain sizes are equivalent to steady state values for the two stages. Recrystallized grain size piezometry could be effectively carried out on these samples and yield reasonable stress estimates for both deformation stages. B. Samples experiencing a stress decrease followed by either continued strain (black line) or no strain (thick grey line). Grain growth involves formation of a foam or partial-foam texture (Figs. 3 and 4b). Grain size from a partial foam texture puts an upper limit on the stress of the second stage of deformation and a lower limit on the earlier stress.

2010; Bestmann et al., 2012). For example, Twiss (1977) predicted that even at a constant stress, a certain amount of strain is needed before a steady state recrystallized grain size is reached. Alternatively, for our experiments we find that quantitative information regarding stress can be extracted from the microstructures of our samples regardless of whether stress was changing or a microstructural steady state had been reached.

For the experiments involving a significant stress decrease, we find that when coupled with microstructural observations, recrystallized grain size provides a constraint on the final stress at the time of quenching and sometimes also on earlier stress levels. For example, following regime 1 deformation at high stress (grey shaded area in Fig. 1), grain size in most samples kept pace with gradual (w1515, w1516, w1527) or even abrupt (w1524, w1710) decreases in stress. As a result, these samples plot on the piezometer (Fig. 1), although one sample (w1516) also shows a finer grain size in a lower strain region consistent with a stress from an earlier period. Samples that experienced major decreases in stress just prior to quenching (w1524, w1710) or that have recrystallized grain sizes significantly smaller than expected at steady state for the stress they were experiencing just prior to quenching (w1518, w1522) have foam or partial foam textures. Previous analyses indicate that foam textures (Figs. 3a and 7d) are expected after a major stress decrease (e.g. Tullis and Yund, 1982; Hacker et al., 1990, 1992; Masuda et al., 1997; Heilbronner and Tullis, 2002). Applying the piezometer to samples with a foam texture gives a stress lower than the peak stress experienced prior to the stress decrease and higher than the stress experienced just prior to quenching. The grain size associated with a partial foam texture (e.g. Figs. 3b, 4d and 7c) indicates a stress value either equivalent to the final stress (w1524, w1710) or slightly below it (w1518). For all of the experiments involving a decrease in stress, an analysis of grain size coupled with microstructural observations provides a quantitative constraint on stress history.

During a significant stress increase, we find that recrystallized grains form at their steady state grain size, i.e. at the size indicated by the piezometer for the stress they are experiencing (Fig. 9). For example, after only small amounts of recrystallization (e.g. w1509) and regardless of deformation history (compare w1509, w1515 and w1527; Fig. 2), high stress samples have recrystallized grain sizes equivalent to those generated during extended, steady state experiments on fine-grained novaculite (Fig. 1). A strain-invariant recrystallized grain size in quartz is also suggested by the results

of Heilbronner and Tullis (2006) for general shear experiments (shear strains up to ~8). Similarly, Kidder et al. (2012) found that recrystallized grains in very slightly recrystallized rocks from Taiwan indicate stress magnitudes that match independent constraints on long-term stress values in the region. We conclude that recrystallized grain size provides a reliable constraint on the most recent stress experienced.

For samples with a pre-existing population of recrystallized grains from an initial low stress stage of deformation, a bimodal distribution of recrystallized grain size develops (Fig. 5). In this case, the distinct populations of recrystallized grains reveal the two-stage deformation history. Analogous microstructures are common in natural samples (e.g. Dunlap et al., 1997; Little et al., 2002; Behr and Platt, 2011; Kidder et al., 2012, 2013).

Overall, our observations (summarized in Fig. 13) suggest that accurate paleostress estimates can be obtained for samples that experienced only minor amounts of recrystallization and in some situations where samples did not experience extended periods of steady state creep. If the microstructures produced in the experiments involving significant stress changes were encountered in a suite of naturally deformed samples: 1) We would correctly estimate the stress during the final stage of deformation for at least four of the samples (w1509, w1515, w1525, w1526). For two of these samples (w1509, w1515) observations of older, coarse recrystallized grains (e.g. Fig. 5) could be used to estimate the lower stress associated with earlier deformation. 2) For the three samples with partial foam textures, we would recognize deformation under conditions of decreased stress. For two of these samples (w1524, w1710), piezometric analysis would provide a correct estimate of the final stress. For the other (w1518), the grain size analysis would overestimate the final stress by approximately a factor of two. 3) The two grain sizes measured in sample w1516 would indicate two points on the stress path and it would remain somewhat ambiguous whether stress increased or decreased. However, the occurrence of coarser recrystallized grains in the highest strain region would suggest a decrease to a value equivalent to the final stress. 4) In sample w1522, the foam texture would indicate a stress drop to nominally isostatic conditions and provide a minimum constraint on peak stress. Thus, in all the samples with complicated deformation histories, a microstructural analysis coupled with grain size piezometry would provide accurate constraints on stress history. Final stress would be estimated accurately ($\pm 20\%$) in eight of the nine samples, including the samples (w1524, w1710) where the second

stage was associated with minimal strain <3%.

5.2. Mechanisms of grain growth during dynamic recrystallization

A key assumption of several grain-size evolution models (e.g. De Bresser et al., 1998; Hall and Parmentier, 2003; Austin and Evans, 2007) is that a balance of grain size reduction and grain growth determines the average size of grains during deformation. It is assumed in these models that grain growth rates during dynamic recrystallization can be approximated using relationships derived from isostatic grain-growth experiments, i.e. that during dynamic recrystallization grain growth mainly results from a minimization of grain-boundary surface energy. Both our microstructural observations and observed growth rates support this assumption.

Platt (2015) argued that the achievement of a steady-state grain size based on a balance between grain growth and reduction is unlikely because the grain-boundary topologies of the two processes result in opposite radii of curvature. However, we observe: (1) triple junctions indicative of surface-energy driven grain growth in samples undergoing both deformation after a stress decrease (Figs. 3 and 4b) and constant stress (Fig. 4a); and (2) that these triple junctions are more abundant in the samples where stress was lowered than in samples experiencing constant stress (e.g. Figs. 3b and 4). These observations suggest that increases in recrystallized grain size during deformation are at least partly driven by grain-boundary surface energy. The presence of triple junctions with an annealed appearance in steady state samples (e.g. Fig. 4a) suggests that surface energy driven growth is also involved in maintaining steady state recrystallized grain size. Based on the observation of local variations in recrystallized grain size (Fig. 10), we postulate that grain size undergoes local oscillations of growth and reduction, perhaps in response to shifting stress chains (e.g. Peters et al., 2005).

The importance of surface energy-driven grain growth is also supported by grain growth rates during our experiments. Recrystallized grain sizes in the five experiments where stress was lowered (w1518, w1522, w1524, w1526 and w1710) all fall near the static growth curve (Fig. 12). Grain growth thus appears to occur at similar rates in (a) isostatic experiments on undeformed quartz, (b) deformed quartz undergoing annealing, and (c) deformed quartz undergoing continued deformation at a new lower stress state (Fig. 12). Growth of grains in hard orientations (Fig. 8) suggests that grain-boundary migration during growth was partly driven by gradients in dislocation density (Gleason et al., 1993), however this behavior does not appear to significantly affect overall grain growth rates. In summary, our observations of growth rates and microstructures suggest that grain-boundary surface energy is an active driver of grain-growth during dislocation creep, and therefore that it is appropriate, at least to a first order, to incorporate static grain-growth relationships in piezometric relationships.

5.3. The wattmeter

5.3.1. Applicability of the wattmeter to partially recrystallized samples

As emphasized above, the wattmeter predicts average grain size (Austin and Evans, 2009) and thus, strictly, only predicts recrystallized grain size after samples achieve microstructural steady state (i.e., after 100% recrystallization). This point merits clarification because Austin and Evans (2007) mistakenly plotted the recrystallized grain size data of Stipp and Tullis (2003) in their Fig. 2 (similar to our Fig. 11b) instead of average grain size. We are, however, struck by the close match between observed recrystallized grain sizes and the average grain sizes predicted by the

wattmeter (Figs. 11b and 12). The match is particularly compelling given that the stress-grain size data for quartz require separate piezometers to fit the high and low stress data (Fig. 1; Stipp and Tullis, 2003), and that some of our data were acquired at conditions where the grain size was evolving. We deduce that the values are similar because recrystallized grain size quickly reaches a value consistent with ambient deformation conditions, i.e. at a given stress, recrystallized grain size will be approximately the same regardless of the extent of recrystallization. Evidence for this is provided by comparison of samples that experienced different strains at similar stress conditions, e.g. Stipp et al. (2010) noted that recrystallized grain size is “almost fully established after only a few percent axial strain.” Similarly, Fig. 9 shows no correlation between the stress-recrystallized grain size relationship and strain, even for the two-stage experiments. These observations suggest that the size of recrystallized grains is mainly determined by ambient stress, and thus provide a justification for comparing steady-state grain sizes predicted by the wattmeter with recrystallized grain sizes in partially recrystallized samples (e.g. Fig. 11b).

5.3.2. Predicted and observed grain-size reduction rates

While the wattmeter predicts grain-sizes that closely match recrystallized grain size for quartz, it significantly over-predicts aggregate grain-size reduction rates. The average grain size in our experiments is significantly larger than predicted by the wattmeter, particularly for samples with small recrystallized grains (Figs. 11b and 12). This difference translates to observed average grain size reduction rates (Table 1) that are about an order of magnitude slower than predicted (Fig. 12). How does the wattmeter manage to accurately strike the balance of growth and reduction rates in recrystallized regions (e.g. filled symbols in Fig. 11b) if overall grain size reduction rates are so erroneous?

The value of λ (the fraction of the power input stored in the material microstructure; Eq. (1)) is the largest source of uncertainty in the wattmeter. Austin and Evans (2007, 2009) proposed a value of $\lambda \approx 0.1$ based on comparisons to experimental data, but they emphasize that it should not be considered a constant – and suggest that λ may be dependent on dislocation density and/or recrystallization mechanism. Empirically, the observation that the wattmeter does a good job of predicting recrystallized grain size indicates that the grain-size reduction rate within recrystallized regions is well predicted by the wattmeter with $\lambda \sim 0.1$. In contrast, the grain-size reduction rate of porphyroclasts, which determines the relationship between strain and percent recrystallization (e.g. Heilbronner and Tullis, 2006; Muto et al., 2011), is substantially smaller than predicted by Austin and Evans (2007).

We suggest that consideration of micro-scale processes associated with dynamic recrystallization (and how they relate to λ , dissipation rate and β (the wattmeter term describing the fraction of work rate accommodated by dislocation creep); Eq. (1)) can explain why the wattmeter over-predicts the overall grain-size reduction rates. Microstructural observations indicate that during deformation in regimes 2 and 3, the porphyroclasts and recrystallized grains deform at similar rates (i.e., deformation is not grain size dependent), and hence that the product of stress and dislocation creep strain rate is similar in recrystallized areas and porphyroclasts (with $\beta = 1$, Eq. (1)). Thus, the slower-than-expected “porphyroclast reduction rate” suggests that λ is smaller for the porphyroclasts than the recrystallized matrix. Lower values of λ in porphyroclasts may arise where the creation of a recrystallized matrix allows for more uniform strain rates in the surviving porphyroclasts—owing to a relaxation of grain boundary strain compatibility constraints, which in turn would decrease the rate of subgrain boundary formation. Herwegh et al. (2014) suggested that data from deformation experiments on calcite are best fit by a

Table 1
Experimental data. Abbreviations: ϵ , strain; $\dot{\epsilon}$, strain rate; σ , differential stress; rxld, recrystallized; g.s., grain size; hs, high strain zone; RMS, Root Mean Square, subscripts “1” and “2” refer to stages one and two of the experiments. Reported stresses are either averages over the interval between 10% strain and the final stress, or final stresses (w1509, w1515, w1516, w1522, w1524, w1527, w1710; see text for details). Temperature was maintained at 900 °C during all the experiments except w1524 (see text). Grain size reduction rates reflect the difference between initial (~70 μm) and final average grain sizes.

Experiment	$\dot{\epsilon}_1$ (s^{-1})	$\dot{\epsilon}_2$ (s^{-1})	ϵ_{Total}	ϵ_2	σ (MPa)	N	Median rxld g.s. (μm)	RMS rxld g.s. +/- std error	N	RMS g.s. (μm) +/- std error	g.s. reduction rate ($\mu\text{m s}^{-1}$)
w1341	1.48–2.86E-5	NA	48.4	NA	242	281	2.37	3.57 + 0.27 – 0.07	135	19.36 + 0.78 – 0.07	1.37E-03
w1505	1.45–1.94E-6	NA	25.1	NA	100 ± 15	398	8.46	10.10 + 0.73 – 0.19	496	19.21 + 1.05 – 0.19	2.94E-04
w1509	1.44–1.75E-6	1.75–2.32E-4	37.9	20.3	813	255	1.13	1.63 + 0.13 – 0.04	101	24.89 + 1.69 – 0.07	2.85E-02
w1510	1.45–3.09E-6	NA	53.2	NA	87 ± 16	1794	5.53	7.37 + 0.24 – 0.06	1817	7.98 + 0.25 – 0.06	1.79E-04
w1515	1.44–1.97E-6	3.94–5.82E-5	59.1	32.3	597	578	1.29	1.64 + 0.09 – 0.03	209	6.89 + 0.17 – 0.03	3.37E-04
w1516	2.88–5.78E-5	NA	53.0	NA	416	384	1.14	1.57 + 0.10 – 0.03	134	10.23 + 0.33 – 0.03	5.52E-03
w1516hs	>2.88–>5.78E-5	NA	>53.0	NA	416	260	1.50	1.90 + 0.16 – 0.05	125	5.69 + 0.30 – 0.05	5.94E-03
w1518	2.88–4.01E-5	2.00–2.37E-6	43.6	15.5	58 ± 3	508	7.47	9.48 + 0.60 – 0.14	540	11.83 + 0.68 – 0.14	7.02E-04
w1522	2.91–4.13E-5	~4.8–<4.8E-7	33.6	4.0	1	646	6.75	9.91 + 0.52 – 0.12	657	10.88 + 0.55 – 0.12	6.94E-04
w1524	2.92–4.14E-5	2.07–2.13E-6	32.4	2.8	337	397	1.67	2.18 + 0.14 – 0.05	114	17.09 + 0.80 – 0.06	2.76E-02
w1525	1.43–1.94E-6	3.88–5.04E-5	49.5	23.0	192 ± 7	1138	2.30	3.39 + 0.13 – 0.03	122	12.97 + 0.81 – 0.09	3.00E-04
w1526	1.45–1.91E-5	1.91–2.58E-6	50.0	26.0	124 ± 15	426	8.83	10.60 + 0.76 – 0.18	516	16.07 + 0.96 – 0.18	3.26E-04
w1527	2.87–4.18E-5	NA	31.2	NA	680	126	1.11	1.52 + 0.17 – 0.06	118	32.41 + 2.71 – 0.08	6.59E-03
w1710	2.89–4.1E-5	2.05–2.11E-6	32.5	2.8	340	272	1.41	1.93 + 0.15 – 0.05	100	31.00 + 2.05 – 0.07	2.03E-02

gradual increase in λ . At face value, this interpretation is consistent with our suggestion that λ is different for porphyroclasts and recrystallized grains, as an increase in the fraction of recrystallized grains with increasing strain would result in an increase in the average value of λ .

During deformation in regime 1, the porphyroclasts initially work harden and strain localizes in the weaker, recrystallized matrix. Here, a lower porphyroclast reduction rate is qualitatively explained by a decreased dissipation rate within porphyroclasts—owing to the lower strain rate—and potentially a decrease in β (see Section 5.4).

5.3.3. Extrapolation of the wattmeter to low temperatures

Extrapolation of the wattmeter to natural, low-temperature deformation conditions yields poor results, at least as currently formulated using the flow law of Hirth et al. (2001) and grain growth relationship of Wightman et al. (2006). The inconsistency is illustrated using the data of Dunlap et al. (1997) from the Ruby Gap Duplex, Australia. The flow law of Hirth et al. (2001) is calibrated using the thermochronologically constrained temperature and strain rates from the Ruby Gap Duplex and based partly on the premise that a stress of 100 MPa is associated with the observed recrystallized grain size there of 20–40 μm . Application of the wattmeter predicts stresses an order of magnitude lower (4–13 MPa) for the observed grain size and deformation temperature (250–350 °C). In a Taiwanese quartzite deformed at similarly low temperatures, Kidder et al. (2012) also found that the stresses based on the wattmeter were about an order of magnitude lower than several independent estimates of stress. We hypothesize that this discrepancy arises from applying a quartz grain–growth relationship that is too sluggish when extrapolated to low temperatures. This explanation is supported by Cross et al. (2015) and Wightman et al. (2006), who found that grain growth rates in nature are likely greater than predictions based on the experimental quartz grain–growth relationship. Our experiments were carried out at similar conditions as the grain growth experiments, so this issue does not complicate our analysis.

5.4. A Newtonian viscosity for regime 1?

The behavior of quartzite deformed experimentally in dislocation creep regimes 2 and 3 fits an equation of the form,

$$\dot{\epsilon} = A\sigma^n e^{(-Q/RT)} \quad (2)$$

where $\dot{\epsilon}$ is strain rate, A is a material constant, σ is differential stress (MPa) raised to an exponent $n = 3–4$, Q is the creep activation energy (kJ mol^{-1}), R is the gas constant, and T is absolute temperature (e.g. Paterson and Luan, 1990). The weakening effect of water can be included by adding a fugacity-dependence to the A term (Hirth et al., 2001). A more practical form of the flow law is presented in the Appendix, with the effect of water incorporated through a pressure-dependence of Q rather than a fugacity term.

Quartzite in regime 1 is significantly stronger than predicted by the flow law of Hirth et al. (2001) and the initial strength is grain-size sensitive (Hirth et al., 2001). Additionally, EBSD-data indicate grain-boundary sliding in high strain zones of regime 1 experiments (Stipp and Kunze, 2008). These observations indicate a different type of deformation in regime 1 relative to the other regimes. We are able to estimate n for regime 1 using two methods. First, an estimate of $n \approx 1.5$ for regime 1 can be made using the results of experiment w1518 and the following relationship derived from Eq. (2):

$$n = \frac{\ln \dot{\epsilon}_1 - \ln \dot{\epsilon}_2}{\ln \sigma_1 - \ln \sigma_2} \quad (3)$$

where the subscripts 1 and 2 refer to the time immediately before and after a stress drop. For comparison, Eq. (4) predicts $n = 3.9$ for experiment w1526 (a change from regime 2 to regime 3 conditions), similar to previous estimates in regimes 2 and 3 (e.g. Paterson and Luan, 1990; Hirth et al., 2001). A second estimate of n in regime 1 can be made using the wattmeter. According to the wattmeter, the slope of data on a log stress vs. log recrystallized grain–size plot (e.g. Fig. 1) is $(n + 1)/(p + 1)$, where p is the grain growth exponent (see Eq. (1)). As we have assumed a value for p of 3.2 following Wightman et al. (2006), we calculate a value of $n = 1.0$ for regime 1 and $n = 4.0$ for the regime 2 and 3 data. Both approaches suggest that regime 1 deformation has a nearly Newtonian viscosity. These results suggest that diffusion and grain-boundary sliding become significant deformation mechanisms of very small recrystallized grains in regime 1. We suggest that this change is responsible for the kink in the quartz piezometer (Fig. 1).

Rutter and Brodie (2004) produced a linear-viscous diffusion creep flow law for dry quartz (water fugacity <100 MPa). Their flow law predicts viscosities ($\sim 10^{16}$ Pa s) for our regime 1 experiments,

50–3000 times higher than we observed. This difference might be explained by higher water fugacity in our experiments (~5 GPa) if regime 1 rheology has a similar sensitivity to water fugacity as regime 2 and 3 deformation (Hirth et al., 2001).

6. Conclusions

Ultimately we hope that microstructural observations can be used to fully discern and quantify the potentially wide variety of rheologic behaviors that rocks experience at deep crustal levels. We have demonstrated here that the microstructures associated with a major and sustained change in stress should be recognizable (unless the earlier microstructure was completely overprinted). A change to a lowered stress results in a partial foam texture. A major stress increase leads to a bimodal distribution of recrystallized grains. In both cases, the size of recrystallized grains provides useful, quantitative constraints on stress history.

The experiments provide perspective on the relevance of the wattmeter theory to the grain size evolution of quartz: 1) Microstructural observations and observed grain growth rates support the theoretical underpinnings of the wattmeter as a balance of grain size reduction and “static” growth processes. 2) The wattmeter proves to be a good predictor of recrystallized grain size and grain growth rates during deformation, but significantly overestimates rates of grain size reduction and thus poorly predicts average grain size in partially recrystallized samples. 3) The wattmeter underestimates stress values at low, “geologic” temperatures because the current, experimentally derived static grain–growth relationship is too slow when extrapolated to natural conditions.

Bimodal distributions of recrystallized grains analogous to those developed in our stress increase experiments are common features of many exhumed mylonites, and an important remaining question is whether more complex deformation histories could also produce similar fabrics. In particular, we hypothesize that pulses of high stress associated with earthquakes (e.g. Küster and Stöckhert, 1998) might also be involved in generating bimodal populations of recrystallized grains. For purposes of interpreting the rheologic history of rocks based on their microstructures, it is critical to distinguish between these different scenarios. The experiments and analysis described here provide groundwork for further work toward this goal.

Acknowledgements

The project was supported by the Caltech Tectonics Observatory, the National Science Foundation under Grants IRFP-1064805 to Kidder and EAR-1220075 to Hirth, and the Cohen Foundation of CCNY. Thanks to Eric Goergen and Linda Chernak for patient laboratory instruction, Linda Chernak for the use of sample w1341, and Jan Tullis for helpful discussions. Robin Kidder helped design the figures. L. Montési provided a critical line of code used for the grain size modeling. We also thank A. Cross, D. Prior, and M. Stipp for the use of EBSD maps of three samples, W. Sullivan for a helpful review, and B. Dunne for his editorial work. A thorough review of an early version by M. Stipp led to significant improvements in the manuscript.

Appendix A. Supplementary data

Supplementary data related to this article can be found at <http://dx.doi.org/10.1016/j.jsg.2015.12.004>.

Appendix

A simplified version of the flow law of Hirth et al. (2001) can be

constructed by fitting the relationship between water fugacity ($f_{\text{H}_2\text{O}}$), pressure P (in Pa) and absolute temperature T (Tödde, 1972) with an Arrhenius relationship (Shinevar et al., 2015):

$$f_{\text{H}_2\text{O}} \sim 12000 \cdot \exp(- (35000 - 18e^{-6P}) / (RT))$$

Substituting this relationship into the flow law of Hirth et al. (2001) gives:

$$\dot{\epsilon}' = 7.6e^{-8\sigma^4} \cdot \exp(- (170000 - 18e^{-6P}) / (RT))$$

The negative sign on the activation term arises from the large effect of pressure on water fugacity. This formulation assumes lithostatic fluid pressure and that water is the only fluid phase present. Note also that estimates of $f_{\text{H}_2\text{O}}$ as a function of P and T can also be made using Wither's fugacity calculator: <http://www.esci.umn.edu/people/researchers/withe012/fugacity.htm>.

References

- Austin, N.J., 2011. The microstructural and rheological evolution of shear zones. In: Prior, D.J., Rutter, E.H., Tatham, D.J. (Eds.), *Deformation Mechanisms, Rheology and Tectonics: Microstructures, Mechanics and Anisotropy*. Geological Society, London, pp. 193–209.
- Austin, N.J., Evans, B., 2007. Paleowattmeters: a scaling relation for dynamically recrystallized grain size. *Geology* 35, 343–346.
- Austin, N.J., Evans, B., 2009. The kinetics of microstructural evolution during deformation of calcite. *J. Geophys. Res.* 114.
- Behr, W.M., Platt, J.P., 2011. A naturally constrained stress profile through the middle crust in an extensional terrane. *Earth Planet. Sci. Lett.* 303, 181–192.
- Bestmann, M., Pennacchioni, G., Nielsen, S., Göken, M., de Wall, H., 2012. Deformation and ultrafine dynamic recrystallization of quartz in pseudotachylite-bearing brittle faults: a matter of a few seconds. *J. Struct. Geol.* 38, 21–38.
- Bishop, R.R., 1996. Grain Boundary Migration in Experimentally Deformed Quartz Aggregates: the Relationship between Dynamically Recrystallized Grain Size and Steady State Flow Stress. Brown University, Providence, R.I., p. 36
- Brace, W.F., Kohlstedt, D.L., 1980. Limits on lithospheric stress imposed by laboratory experiments. *J. Geophys. Res.* 85, 6248–6252.
- Bürgmann, R., Ergintav, S., Segall, P., Hearn, E., McClusky, S., Reilinger, R., Woith, H., Zschau, J., 2002. Time-dependent distributed afterslip on and deep below the izmit earthquake rupture. *Bull. Seismol. Soc. Am.* 92, 126–137.
- Chernak, L.J., Hirth, G., Sevlerstone, J., Tullis, J., 2009. Effect of aqueous and carbonic fluids on the dislocation creep strength of quartz. *J. Geophys. Res.* 114, B04201.
- Christie, J.M., Ord, A., 1980. Flow stress from microstructures of mylonites: example and current assessment. *J. Geophys. Res.* 85, 6253–6262.
- Cross, A.J., Kidder, S., Prior, D., 2015. Using quartz sheared around garnet porphyroclasts to evaluate microstructural evolution in nature. *J. Struct. Geol.* 75, 17–31.
- De Bresser, J.H., Peach, C., Reijs, J., Spier, C., 1998. On dynamic recrystallization during solid state flow: effects of stress and temperature. *Geophys. Res. Lett.* 25, 3457–3460.
- De Bresser, J.H., Ter Heege, J.H., Spiers, C.J., 2001. Grain size reduction by dynamic recrystallization: can it result in major rheological weakening? *Int. J. Earth Sci.* 90, 28–45.
- Derby, B., 1990. Dynamic recrystallization and grain size. In: Barber, D.J., Meredith, P.G. (Eds.), *Deformation Processes in Minerals, Ceramics and Rocks*. Unwin Hyman, London, pp. 354–364.
- Derby, B., Ashby, M.F., 1987. On dynamic recrystallization. *Scr. Met.* 21, 879–884.
- Druiventak, A., Matysiak, A., Renner, J., Trepmann, C., 2012. Kick-and-cook experiments on peridotite: simulating coseismic deformation and post-seismic creep. *Terra Nova* 24, 62–69.
- Dunlap, W., Hirth, G., Teysier, C., 1997. Thermomechanical evolution of a ductile duplex. *Tectonics* 16, 983–1000.
- Edward, G.H., Etheridge, M.A., Hobbs, B.E., 1982. On the stress dependence of subgrain size. *Textures Microstruct.* 5, 127–152.
- Fagereng, A., Sibson, R., 2013. Melange rheology and seismic style. *Geology* 38, 751–754.
- Fitz Gerald, J.D., Mancktelow, N.S., Pennacchioni, G., Kunze, K., 2006. Ultrafine-grained quartz mylonites from high-grade shear zones: evidence for strong dry middle to lower crust. *Geology* 34, 369.
- Getsinger, A., Hirth, G., 2014. Amphibole fabric formation during diffusion creep and the rheology of shear zones. *Geology* 42, 535–538.
- Gleason, G.C., Tullis, J., 1993. Improving flow laws and piezometers for quartz and feldspar aggregates. *Geophys. Res. Lett.* 20, 2111–2114.
- Gleason, G.C., Tullis, J., Heidelbach, F., 1993. The role of dynamic recrystallization in the development of lattice preferred orientations in experimentally deformed quartz aggregates. *J. Struct. Geol.* 15, 1145–1168.
- Hacker, B.R., Yin, A., Christie, J.M., Davis, G.A., 1992. Stress magnitude, strain rate, and rheology of extended middle continental-crust inferred from quartz grain sizes in the Whipple Mountains, California. *Tectonics* 11, 36–46.
- Hacker, B.R., Yin, A., Christie, J.M., Snoke, A.W., 1990. Differential stress, strain rate,

- and temperatures of Mylonitization in the Ruby Mountains, Nevada - implications for the rate and duration of uplift. *J. Geophys Res-Solid* 95, 8569–8580.
- Hackl, K., Renner, J., 2013. High-temperature deformation and recrystallization: a variational analysis and its application to olivine aggregates. *J. Geophys. Res.* 118, 1–25.
- Hall, C.E., Parmentier, E.M., 2003. Influence of grain size evolution on convective instability. *Geochim. Geophys. Geosystems* 4.
- Handy, M., Hirth, G., Hovius, N., 2007. Continental Fault Structure and Rheology from the Frictional-to-viscous Transition Downward, Tectonic Faults: Agents of Change on a Dynamic Earth. MIT Press, pp. 139–182.
- Heilbronner, R., Tullis, J., 2002. The effect of static annealing on microstructures and crystallographic preferred orientation of quartzites experimentally deformed in axial compression and shear. In: De Meer, S., Drury, M.R., De Bresser, J.H., Pennock, G.M. (Eds.), *Geol. Soc. Spec. Publ.* 191–218.
- Heilbronner, R., Tullis, J., 2006. Evolution of c axis pole figures and grain size during dynamic recrystallization: results from experimentally sheared quartzite. *J. Geophys. Res.* 111.
- Herwegh, M., Poulet, T., Karrech, A., Regenauer-Lieb, K., 2014. From transient to steady state deformation and grain size: a thermodynamic approach using elasto-visco-plastic numerical modeling. *J. Geophys. Res.* 119, 900–918.
- Hirth, G., Teyssier, C., Dunlap, W., 2001. An evaluation of quartzite flow laws based on comparisons between experimentally and naturally deformed rocks. *Int. J. Earth Sci. (Geol. Rundsch)* 90, 77–87.
- Hirth, G., Tullis, J., 1992. Dislocation creep regimes in quartz aggregates. *J. Struct. Geol.* 14, 145–159.
- Hobbs, B.E., 1968. Recrystallization of single crystals of quartz. *Tectonophysics* 6, 353–401.
- Holyoke, C.W.I., Kronenberg, A.K., 2013. Reversible water weakening of quartz. *Earth Planet. Sci. Lett.* 374, 185–190.
- Kenkmann, T., Dresen, G., 1998. Stress gradients around porphyroclasts: palaeopiezometric estimates and numerical modelling. *J. Struct. Geol.* 20, 163–173.
- Kidder, S.B., Avouac, J.P., Chan, Y.C., 2012. Constraints from rocks in the Taiwan orogen on crustal stress levels and rheology. *J. Geophys. Res.* 117.
- Kidder, S.B., Avouac, J.P., Chan, Y.C., 2013. Application of titanium-in-quartz thermobarometry to greenschist facies veins and recrystallized quartzites in the Shüehshan range, Taiwan. *Solid Earth* 4, 1–21.
- Kidder, S.B., Prior, D., 2014. Reversed scan direction reduces electron beam damage in EBSD maps. *J. Microsc.*
- Kohlstedt, D.L., Evans, B., Mackwell, S.J., 1995. Strength of the lithosphere—constraints imposed by laboratory experiments. *J. Geophys Res-Sol Ea.* 100, 17587–17602.
- Küster, M., Stöckhert, B., 1998. High differential stress and sublithostatic pore fluid pressure in the ductile regime — microstructural evidence for short-term post-seismic creep in the Sesia Zone, Western Alps. *Tectonophysics* 199, 263–277.
- Little, T., Holcombe, R.J., Ilg, B.R., 2002. Ductile fabrics in the zone of active oblique convergence near the Alpine Fault, New Zealand: identifying the neotectonic overprint. *J. Struct. Geol.* 24, 193–217.
- Lopez-Sanchez, M.A., Llana-Funez, S., 2015. An evaluation of different measures of dynamically recrystallized grain size for paleopiezometry or paleowattometry studies. *Solid Earth* 6, 475–495.
- Lowry, A.R., Pérez-Gussinyé, M., 2011. The role of crustal quartz in controlling Cordilleran deformation. *Nature* 471, 353–357.
- Mancktelow, N.S., Pennacchioni, G., 2004. The influence of grain boundary fluids on the microstructure of quartz-feldspar mylonites. *J. Struct. Geol.* 26, 47–69.
- Masuda, T., Morikawa, T., Nakayama, Y., Suzuki, S., 1997. Grain-boundary migration of quartz during annealing experiments at high temperatures and pressures, with implications for metamorphic geology. *J. Metamorph. Geol.* 15, 311–322.
- Means, W.D., 1989. Synkinematic microscopy of transparent polycrystals. *J. Struct. Geol.* 11, 163–174.
- Menegon, L., Nasipuri, P., Stünitz, H., Behrens, H., Ravna, E., 2011. Dry and strong quartz during deformation of the lower crust in the presence of melt. *J. Geophys. Res.* 116, B10410.
- Mercier, J.-C.C., Anderson, D.A., Carter, N.L., 1977. Stress in the lithosphere: Inferences from steady state flow of rocks. *Pure Appl. Geophys.* 115, 199–226. PAGEOPH.
- Muto, J., Hirth, G., Heilbronner, R., Tullis, J., 2011. Plastic anisotropy and fabric evolution in sheared and recrystallized quartz single crystals. *J. Geophys. Res.* 116.
- Ord, A., Christie, J.M., 1984. Flow stresses from microstructures in mylonitic quartzites of the Moine Thrust zone, Assynt area, Scotland. *J. Struct. Geol.* 6, 639–654.
- Paterson, M.S., Luan, F.C., 1990. Quartzite rheology under geological conditions. In: Knipe, R.J., Rutter, E.H. (Eds.), *Deformation Mechanisms, Rheology and Tectonics*, pp. 299–307. Geological Society Special Publication No. 54.
- Peters, J.F., Muthuswamy, M., Wibowo, J., Tordesillas, A., 2005. Characterization of Force Chains in Granular Material. *Physical Review E* 72, 041307.
- Platt, J.P., 2015. Influence of shear heating on microstructurally defined plate boundary shear zones. *J. Struct. Geol.* 79, 80–89.
- Platt, J.P., Behr, W.M., 2011. Grain size evolution in ductile shear zones: Implications for strain localization and the strength of the lithosphere. *J. Struct. Geol.* 33, 537–550.
- Poirier, J.P., Guillope, M., 1979. Deformation induced recrystallization of minerals. *Bull. De Mineral.* 102, 67–74.
- Prior, D.J., Knipe, R.J., Handy, M.R., 1990. Estimates of the rates of microstructural changes in mylonites. *Deformation mechanisms, rheology and tectonics. Geol. Soc. Spec. Publ.* 54, 309–319.
- Ranalli, G., 1984. Grain size distribution and flow stress in tectonites. *J. Struct. Geol.* 6, 443–447.
- Ross, J.V., Ave Lallemand, H.G., Carter, N.L., 1980. Stress dependence of recrystallized-grain and subgrain size in olivine. *Tectonophysics* 70, 39–61.
- Rozel, A., Ricard, Y., Bercovici, D., 2011. A thermodynamically self-consistent damage equation for grain size evolution during dynamic recrystallization. *Geophys. J. Int.* 184, 719–728.
- Rutter, E.H., Brodie, K.H., 2004. Experimental grain size-sensitive flow of hot-pressed Brazilian quartz aggregates. *J. Struct. Geol.* 26, 2011–2023.
- Shimizu, I., 2008. Theories and applicability of grain size piezometers: the role of dynamic recrystallization mechanisms. *J. Struct. Geol.* 30, 899–917.
- Shinevar, W.J., Behn, M.D., Hirth, G., 2015. Compositional dependence of lower crustal viscosity (In press).
- Stipp, M., Fügenschuh, B., Gromet, L.P., Stünitz, H., Schmid, S.M., 2004. Contemporaneous plutonism and strike-slip faulting: a case study from the Tonale fault zone north of the Adamello pluton (Italian Alps). *Tectonics* 23.
- Stipp, M., Kunze, K., 2008. Dynamic recrystallization near the brittle-plastic transition in naturally and experimentally deformed quartz aggregates. *Tectonophysics* 448, 77–97.
- Stipp, M., Stünitz, H., Heilbronner, R., Schmid, S.M., 2002. The eastern Tonale fault zone: a 'natural laboratory' for crystal plastic deformation of quartz over a temperature range from 250 to 700 °C. *J. Struct. Geol.* 24, 1861–1884.
- Stipp, M., Tullis, J., 2003. The recrystallized grain size piezometer for quartz. *Geophys. Res. Lett.* 30, 2088.
- Stipp, M., Tullis, J., Behrens, H., 2006. Effect of water on the dislocation creep microstructure and flow stress of quartz and implications for the recrystallized grain size piezometer. *J. Geophys. Res.* 111, 1–19.
- Stipp, M., Tullis, J., Scherwath, M., Behrmann, J.H., 2010. A new perspective on paleopiezometry: dynamically recrystallized grain size distributions indicate mechanism changes. *Geology* 38, 759–762.
- Stünitz, H., 1998. Syndeformational recrystallization — dynamic or compositionally induced? *Contributions Mineralogy Petrology* 131, 219–236.
- Tödeheide, K., 1972. Water at high temperature and pressure. In: Franks, F. (Ed.), *Water: A Comprehensive Treatise*, pp. 463–514.
- Toy, V.G., Prior, D.J., Norris, R.J., 2008. Quartz fabrics in the Alpine fault mylonites: Influence of pre-existing preferred orientations on fabric development during progressive uplift. *J. Struct. Geol.* 30, 602–621.
- Trepmann, C., Stöckhert, B., 2001. Mechanical twinning of jadeite - an indication of syneismic loading beneath the brittle-plastic transition. *Int. J. Earth Sci. (Geol. Rundsch)* 90, 4–13.
- Trepmann, C., Stöckhert, B., Dorner, D., Moghadam, R., Kuster, M., Roller, K., 2007. Simulating coseismic deformation of quartz in the middle crust and fabric evolution during postseismic stress relaxation — An experimental study. *Tectonophysics* 442, 83–104.
- Trepmann, C.A., Stöckhert, B., 2003. Quartz microstructures developed during non-steady state plastic flow at rapidly decaying stress and strain rate. *J. Struct. Geol.* 25, 2035–2051.
- Tullis, J., Yund, R.A., 1982. Grain growth kinetics of quartz and calcite aggregates. *J. Geol.* 90, 301–318.
- Tullis, T.E., Tullis, J., 1986. Experimental rock deformation techniques. In: Hobbs, B.E., Heard, H.C. (Eds.), *Mineral and Rock Deformation: Laboratory Studies*. American Geophysical Union, pp. 297–324.
- Twiss, R.J., 1977. Theory and applicability of a recrystallized grain-size paleopiezometer. *Pure Appl. Geophys.* 115, 227–244.
- Urai, J.L., Means, W.D., Lister, G.S., 1986. Dynamic recrystallization of minerals. In: Hobbs, B.E., Heard, H.C. (Eds.), *Mineral and Rock Deformation: Laboratory Studies*, Geophysical Monograph 36, The Paterson Volume. American Geophysical Union, Washington, DC, pp. 161–199.
- Van der Wal, D., Chopra, P., Drury, M., Fitz Gerald, J., 1993. Relationships between dynamically recrystallized grain size and deformation conditions in experimentally deformed olivine rocks. *Geophys. Res. Lett.* 20, 1479–1482.
- Weathers, M.S., Bird, J.M., Cooper, R.F., Kohlstedt, D.L., 1979. Differential stress determined from deformation-induced microstructures of the Moine Thrust zone. *J. Geophys. Res.* 84, 7495–7509.
- White, S., 1977. Geological significance of recovery and recrystallization processes in quartz. *Tectonophysics* 39, 143–170.
- White, S.H., Drury, M.R., Ion, S.E., Humphreys, F.J., 1985. Large strain deformation studies using polycrystalline magnesium as a rock analogue. Part I: grain size paleopiezometry in mylonite zones. *Phys. Earth Planet. Interiors* 40, 201–207.
- Wightman, R., Prior, D., Little, T., 2006. Quartz veins deformed by diffusion creep-accommodated grain boundary sliding during a transient, high strain-rate event in the Southern Alps, New Zealand. *J. Struct. Geol.* 28, 902–918.
- Yund, R.A., Tullis, J., 1982. Grain growth kinetics of quartz and calcite aggregates. *J. Geol.* 90, 301–318.